Hindawi
Advances in Civil Engineering
Volume 2023, Article ID 6690298, 16 pages
https://doi.org/10.1155/2023/6690298

Research Article

Influence of Eggshell Ash and Stone Powder on Geotechnical Properties of Expansive Clay in Dukem Town

Tadesse Endale Teferra,[1] **Eleyas Assefa**,[2] **and S. M. Assefa**[2]

[1]*Mattu University, Metu, Ethiopia*
[2]*Addis Ababa Science and Technology University, Addis Ababa, Ethiopia*

Correspondence should be addressed to Eleyas Assefa; eleyas.assefa@aastu.edu.et

Received 26 May 2023; Revised 13 September 2023; Accepted 26 September 2023; Published 31 October 2023

Academic Editor: Castorina S. Vieira

Expansive clays exhibit a distinctive swelling–shrinkage behavior, leading to structural distress and damage when subjected to varying moisture levels during different seasons. So, to mitigate these issues, stabilization techniques are commonly employed, aiming to diminish swelling tendencies and enhance the strength characteristics of expansive clays. This study delves into the transformative impact of utilizing eggshell ash (ESA) and stone powder (SP) as stabilizing agents on both the index properties and strength parameters of expansive clays. The selection of these stabilizing agents is guided by criteria encompassing cost-effectiveness, availability, and environmental compatibility. Through comprehensive analysis utilizing scanning electron microscopy (SEM) and X-ray diffraction (XRD), the mineralogical compositions of both soil and additives are meticulously examined. The XRD analysis of the expansive clay unveils the presence of minerals such as quartz, sanidine (potassium or sodium feldspar), and magnetite. Incorporating ESA into the expansive clay matrix yields substantial improvements across various soil index values, encompassing the free swell index, free swell ratio, linear shrinkage, and unconfined compressive strength value. To further amplify these benefits, the study extends its focus to the influence of SP while maintaining a consistent 6% ESA content. Notably, the addition of SP exhibits a significant enhancement in compressive strength, alongside other crucial properties. Synthesizing these findings, the laboratory results point to an optimal combination ratio of 6% ESA and 15% SP, as a recommended approach to achieve superior stabilization effects. This research contributes to a deeper understanding of the interplay between stabilizing agents and expansive clays, paving the way for improved engineering practices and more resilient structural designs.

1. Introduction

Expansive clays are predominantly found in regions characterized by arid and semiarid climates, as observed by Vorwerk et al. [1] and Atahu et al. [2]. These clay formations are a result of factors such as inadequate drainage and hot climatic conditions. The unique composition of expansive clays makes them highly problematic, displaying significant changes in volume due to fluctuations in moisture levels. This volumetric behavior is primarily attributed to the presence of montmorillonite clay minerals, as highlighted by Reddy et al. [3]. Furthermore, the relatively weak van der waals forces between silica sheets within these clays contribute to their susceptibility to volume changes upon exposure to moisture variations. Regrettably, this volume fluctuation poses a range of challenges, causing detrimental effects on various structures such as buildings, highway pavements, embankments, and utility lines. Research by Nelson and Miller [4], Canakci et al. [5], and Zada et al. [6] underlines the significant impact of expansive clay-induced damage on infrastructure. In the context of Ethiopia, expansive clays cover an extensive 40% of the land area, presenting a series of threats to vital structures including buildings and roads. Yitagesu et al. [7] and Aga [8] corroborate the widespread presence of expansive clays and their potential consequences. Notably, a significant portion of Dukem town is enveloped by expansive clays, with a prior study by Tamrat [9] revealing an 80% coverage of these clays, characterized by a distinct black hue (CH soil). Within this context, numerous residential buildings, utility lines, and roads in Dukem town exhibit visible signs of damage, manifested in the form of cracks attributed to the swelling and shrinkage tendencies of expansive clays. The detrimental

impact of these clays is underscored by an array of field evidence, highlighting the ongoing and tangible damages they inflict upon residential structures, road networks, utility lines, and various other elements of infrastructure. Removing of such problematic soil and replacing it by an appropriate material or improving it by using chemical or mechanical stabilization are the most commonly adopted stabilization solutions [4, 10]. Traditional stabilizers like lime and cement were widely used to reduce the swelling behavior and improve the strength parameter of expansive clays. However, the traditional stabilizers such as lime, cement, and fly ash are not always preferred due to their adverse effects on the environment since they modify the pH level of treated soil and its surrounding environment [11–13]. In practice, there is a tendency to replace the conventional stabilizers [14] with industrial and agricultural byproducts due to the scarcity of resources and high cost of traditional stabilizers [2, 5]. In a notable investigation conducted by Dang and Khabbaz [13], the shear strength of reinforced soil was explored through the incorporation of 0%–2% Bagasse fiber concentration. Likewise, Atahu et al. [2] undertook a study involving the utilization of 5%–10% coffee husk ash to gauge its impact on the strength and compressibility of expansive clays. In a separate context, Neguse et al. [15] demonstrated that the introduction of 10% enset ash to a weak subgrade soil led to remarkable enhancements in its mechanical properties. The realm of research has witnessed numerous scholars delving into the potential of waste materials, including rice husk ash, coffee husk ash, bagasse ash, rock powder, and eggshell powder [16], as stabilizing agents for the improvement of expansive clays and the concurrent reduction of construction costs. A range of contributions [2, 6, 17–22] have illuminated this avenue. In-depth insights into available stabilization techniques, encompassing both calcium-based and non-calcium-based additives, have been thoughtfully outlined in the comprehensive review presented by Behnood [23]. While a substantial body of research has contributed to our understanding of stabilized soil performance at a macro level examining shear strength, unconfined compressive strength (UCS), and swell behavior, few studies have delved into the intricate microlevel changes within a soil-stabilizer matrix [24]. This gap in knowledge underscores the imperative for innovative soil stabilization analyses at the microlevel. In response to this exigency, the present study is designed to explore the synergistic influence of eggshell ash (ESA) and stone powder (SP) on both the geotechnical properties and microstructure of expansive clay prevalent in Dukem town. This endeavor leverages advanced mineralogical analysis techniques such as X-ray diffraction (XRD) and scanning electron microscopy (SEM) in tandem with conventional index and strength testing methods. The objective is to uncover a holistic understanding of the dual impact of ESA and SP, bridging the gap between macrolevel and microlevel assessments of soil stabilization.

2. Materials and Methods

2.1. Description of Study Area. The research is situated in an expanse characterized by flat topography and limited water drainage, situated approximately 37 km southeast of Addis Ababa. Specifically, the geographic coordinates of the town span roughly from 8°45′25″ to 8°50′30″N latitude and 38°51′55″ to 38°56′5″E longitude. This locale rests at an elevation of 1,950 m above mean sea level, creating an environment where the processes of rock weathering, erosion, and deposition have collaboratively given rise to a substantial accumulation of residual clay and silty-clay soil across the expansive plain of the area.

2.2. Properties of Expansive Clay. In the course of this investigation, a representative soil sample weighing approximately 50 kg was meticulously procured from a depth of 2 m within a test pit located in Dukem town. Following collection, the soil samples were securely packed within plastic bags, ensuring their integrity during transportation to the geotechnical engineering laboratory for subsequent analyses. Upon arrival at the laboratory, the acquired soil sample underwent an air-drying process and was subsequently subjected to sieving utilizing a mesh size of 4.75 mm. To conduct strength assessments, the disturbed soil was meticulously remolded to attain a compaction level of no less than 95% of its maximum dry density, meticulously calibrated to achieve optimal moisture content.

Figure 1 presents the particle size distribution curves for the natural soil, ESA, and SP components. The expansive clay, characterized by its fine-grained, ebony appearance, exhibits an impressive 91.60% passage through the 0.075 mm sieve. Remarkably, the plasticity index (PI) of the expansive clay is prominently close to 50, classifying the soil as CH type inorganic fat clay demonstrating high plasticity. Furthermore, in alignment with AASHTO guidelines, the expansive clay finds its classification within the A-7-5 category, sporting a group index of 20 [25]. Additionally, notable soil characteristics include a free swell index (FSI) of 95% and a corresponding free swelling ratio (FSR) of 1.95. Through the application of the standard compaction test, the expansive clay registers a maximum dry density (MDD) and optimum moisture content (OMC) of 1.32 g/cm^3 and 35.78%, respectively. Impressively, the unconfined compression strength of the soil stands at 95 kPa, bearing testimony to its inherent robustness.

The XRD analysis of the expansive clay offers valuable insights into its mineral composition, revealing a predominant presence of quartz, sanidine (potassium or sodium feldspar), and magnetite minerals (Figure 2). Notably, the distinctive peak corresponding to quartz emerges prominently at $2\theta = 26.62929°$ or $d = 3.344789806$ Å, manifesting as a sharply defined peak. This characteristic peak signifies the high degree of crystallinity within the SiO_2 phase, closely aligning with values observed in the JCPDS (046-1045) standard data. Moreover, the SEM image captures the visual essence of the natural soil, showcasing a diverse amalgamation of angular and nearly rounded particles. Intriguingly, interspersed among these particles are fines, punctuating the mass with void spaces, yielding a heterogeneous and textured appearance (Figure 2).

2.3. Properties of Eggshell Ash. The eggshells employed in this research were sourced from a variety of everyday egg

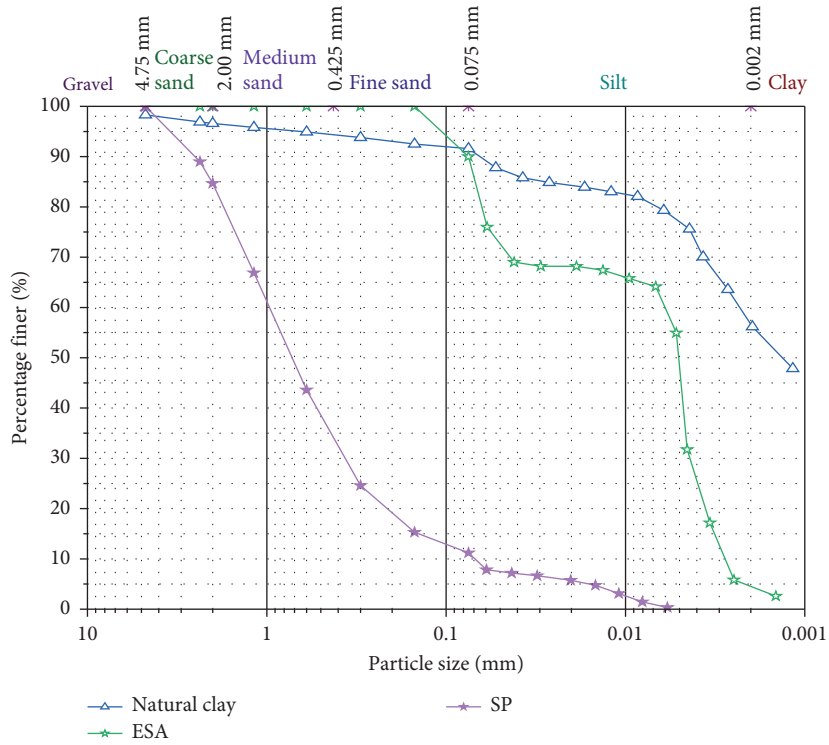

Figure 1: Grain size distribution curve of materials used for the study.

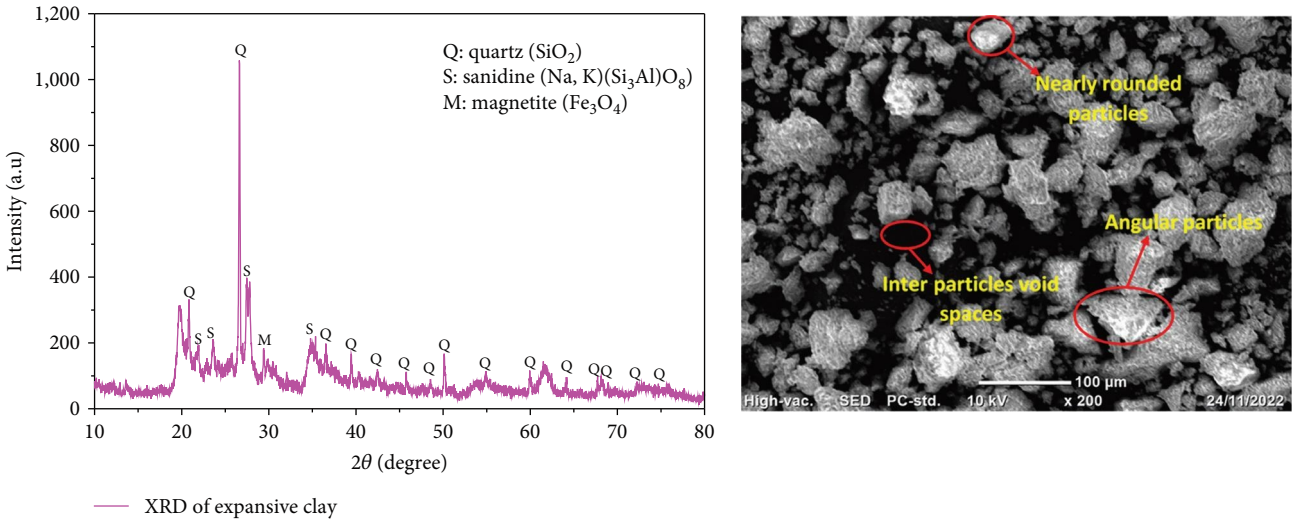

Figure 2: Image plots for expansive clay (a) XRD pattern result and (b) SEM photograph.

consumption, including domestic households, fast-food establishments, and local poultry farms. These collected eggshells, accompanied by their inner delicate membranes, underwent a meticulous purification process to eliminate impurities, subsequently undergoing milling to facilitate the forthcoming combustion procedure. The ESA was generated through a precise calcination process, meticulously executed under controlled conditions at a temperature of $650 \pm 25°C$ for duration of 3 hr within a muffle furnace. Upon completion of the calcination process, the resulting ash was once again subjected to meticulous milling, followed by a sieving procedure with a mesh size of 150 μm. This deliberate refinement process yielded the finely powdered ash material, meticulously tailored for use in this study. Figure 3 offers a comprehensive visual representation of the successive stages involved in the meticulous preparation of ESA, showcasing the exacting steps undertaken.

The specific gravity of the ESA was determined to be 2.55. The chemical composition of the ash is meticulously

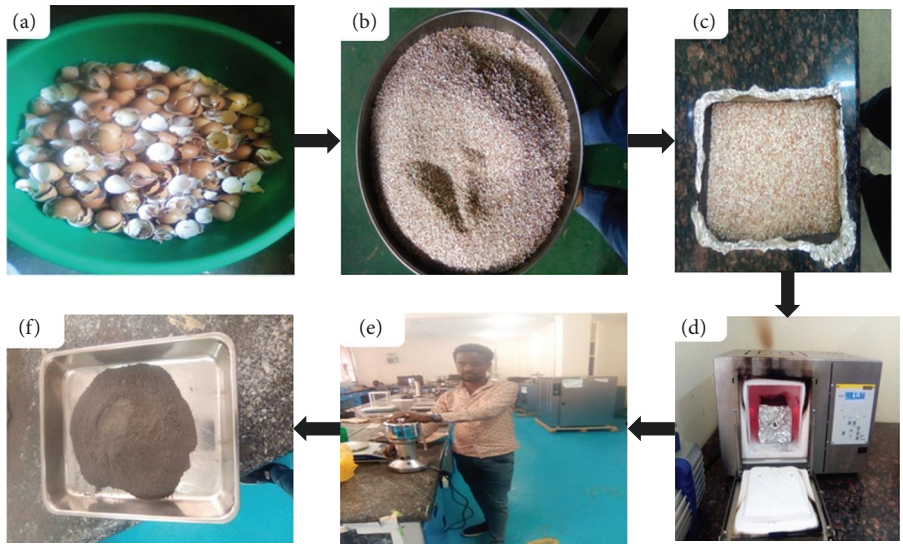

Figure 3: ESA preparation process (a) raw eggshell, (b) ESP, (c) prepared ESP for burning, (d) calcination process, (e) milling of calcined ESA, and (f) sample used for the study.

Table 1: Chemical composition of ESA.

Chemical	Composition (%)
Calcium oxide (CaO)	74.61
Calcium carbonate ($CaCO_3$)	14.79
Magnesium oxide (MgO)	1.39
Silicon dioxide (SiO_2)	0.24
Potassium oxide (K_2O)	0.087
Iron oxide (FeO)	0.0051
Sodium (Na)	0.13
Sulfate (SO_4^{2-})	0.27
Strontium oxide (SrO)	0.13
Nickel oxide (NiO)	0.001
Chlorine (Cl)	0.08
LOI	8.27

detailed in Table 1, revealing a predominant content of 74.61% CaO. The residual fraction encompasses additional elements including MgO, SiO_2, K_2O, FeO, Na, SO_4^{2-}, and assorted minerals, each contributing to the overall composition in varying proportions.

The XRD analysis of the ESA presents a comprehensive insight into its mineral composition, unequivocally revealing the exclusive presence of calcite minerals, as visually depicted in Figure 4. The hallmark peak of calcite, noted at $2\theta = 29.53535°$ or $d = 3.021966351$ Å, emerges as a distinctly sharp feature, attesting to the crystallinity of the calcite phase. This finding concurs closely with values documented in the JCPDS (005-0586) standard data, reaffirming the robust crystalline nature of the calcite. In a parallel study conducted by Tchuente et al. [19], an analogous exploration underscored the composition of ESA, highlighting a substantial calcite mineral content of approximately 96.36%. Complementing this mineralogical characterization, the SEM image, as illustrated in Figure 4(b), offers a captivating depiction of the ESA. This portrayal reveals an intriguing amalgamation of plate-like and finely particulate elements, interspersed with void spaces that punctuate the overall mass.

2.4. Properties of Stone Powder. The SP was sourced from a local crusher site in proximity to Adama city, carefully collected and subsequently subjected to meticulous laboratory preparations in accordance with requisite standards. After collection, the sample underwent a thorough drying process, and particles that successfully passed through a 425 μm sieve were meticulously selected as the material for the ensuing stabilization experiments. A visual representation of the materials harnessed for this study is aptly depicted in Figure 5.

The SP exhibits a specific gravity of 2.78, and the refined powder sample passing through a 425 μm sieve was exclusively utilized. Noteworthy is the particle size distribution test outcome, revealing a mere 11.20% of particles finer than 75 μm sieve. This contrasts the significantly higher percentages of 91.60% for expansive clay and 90% for ESA. Furthermore, in line with AASHTO classification standards, the SP was categorized into the A-3 material group, boasting a commendable zero group index. Figure 6 presents both the SEM photograph and the XRD outline of the SP. The XRD pattern indicates an evident peak intensity spanning the 20°–30° range, indicative of the presence of Cristobalite (SiO_2). This is underlined by the characteristic peaks of cristobalite, notably at $2\theta = 21.93702°$ or $d = 4.048468941$ Å and $2\theta = 27.72983°$ or $d = 3.214491052$ Å, exhibiting sharp peaks denoting pronounced crystallinity. These findings closely correspond with values obtained from the JCPDS (039-1425) standard data, with indications of opal or silicate hydrate occurring beyond this range. In congruence with Blayi et al. [20], the XRD results affirm the significant presence of SiO_2 in SP, approximately 70.02% manifesting as both quartz and silicate hydrate. The SEM photograph in Figure 6(b) presents a captivating depiction of the SP,

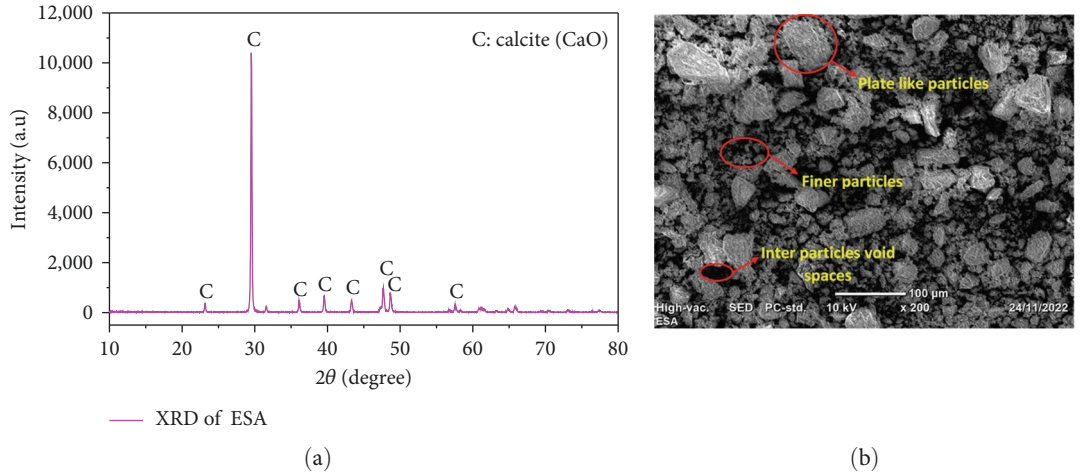

(a) (b)

Figure 4: Image plots of eggshell ash (a) XRD pattern result and (b) SEM photograph.

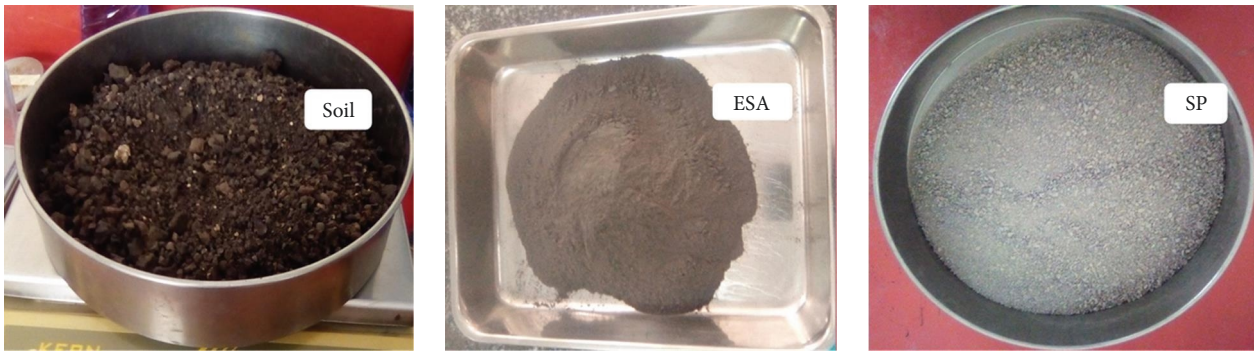

Figure 5: Materials used for the study.

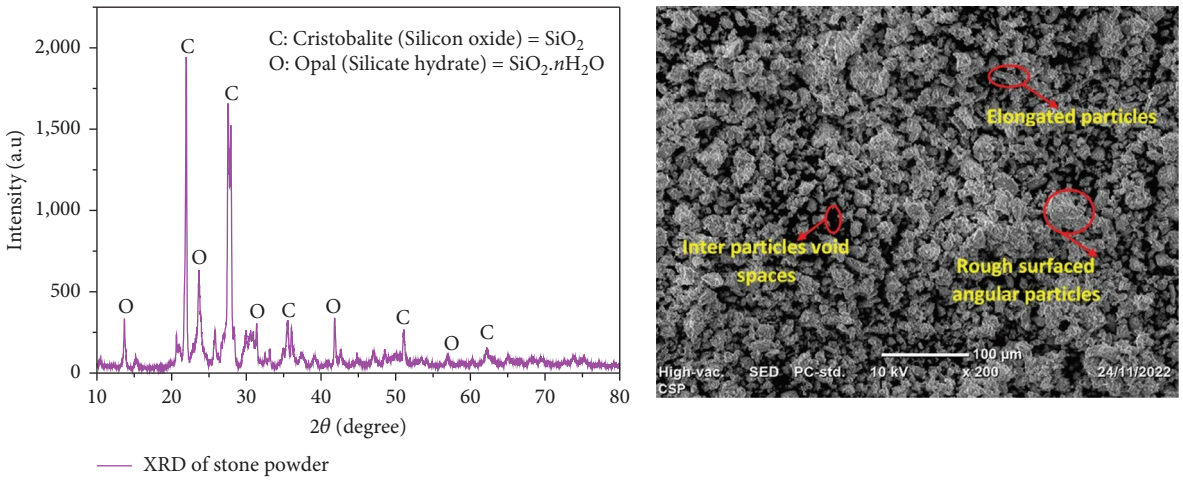

(a) (b)

Figure 6: Image plots for stone powder (a) XRD of SP and (b) SEM photograph.

revealing a mixture of elongated or rod-like particles, adorned with a rough surface, alongside angular particles. Notably, the cumulative composition of Al_2O_3, SiO_2, and Fe_2O_3 in CSP, amounting to 85.27%, satisfies the requisites specified by ASTM C 618 (2000) with regard to the minimum 70% threshold.

Data presented in Table 2 are a comprehensive overview of the material properties for expansive clay, ESA, and SP accompanied by their respective standard testing methods.

2.5. Mix Design. The laboratory analysis conducted aims to unravel the impact of ESA and SP on both the mechanical

Table 2: Summary of geotechnical properties of materials used for the study.

Geotechnical properties	Values			Standard methods
	Soil	ESA	SP	
Natural moisture content (%)	26.68	NA	NA	ASTM D2216
Optimum moisture content (%)	35.78	NA	NA	ASTM D698
Maximum dry density (g/cm^3)	1.32	NA	NA	ASTM D698
Liquid limit (%)	84.38	18.95	16.49	ASTM D4318
Plastic limit (%)	37.22	16.03	NA	ASTM D4318
Plasticity index (%)	47.16	2.92	NA	ASTM D4318
Linear shrinkage (%)	21.96	2.38	1.55	BS 1377-2
Free swell index (%)	95	0.50	0.20	IS 2720-40
Free swell ratio (%)	1.95	1.01	1	IS 2720-40
% Finer of No. 200 sieve (%)	91.60	90	11.20	ASTM D6913
USCS soil classification	CH	ML	SW	ASTM D2487
AASHTO soil classification	A-7-5 (20)	A-4 (0)	A-3 (0)	AASHTO M145
Specific gravity, G_s	2.61	2.55	2.78	ASTM D854
UCS (kPa)	95	NA	NA	ASTM D2166
Compressibility index, C_C	0.62	NA	NA	ASTM D2435
m_v (Mpa^{-1})	0.40	NA	NA	ASTM D2435
Cv (m^2/year)	1.27	NA	NA	ASTM D2435
Color	Black	Dark gray	Dark silver	–

properties and microstructural characteristics of expansive clay. To accomplish this objective, the initial step involved by blending the expansive clay with varying concentrations of ESA namely, 2%, 4%, 6%, and 8%. A meticulous series of laboratory tests were subsequently executed to determine the optimal ESA concentration, primarily gauging its efficacy in enhancing the soil's strength. Based on the conclusive experimental findings, the optimal concentration was determined to be 6% ESA. Building upon this preliminary treatment, the expansive clay, now enriched with 6% ESA, underwent further enhancement through the addition of SP at concentrations of 5%, 10%, 15%, and 20%. This dual addition strategy aimed to uncover the collective influence of these additives on the expansive clay's behavior. The intricate mix design employed for this experimentation is elucidated in Table 3. In essence, this laboratory study embarks on an insightful journey to ascertain the synergistic effects of ESA and SP on both the macroscopic mechanical attributes and the underlying microstructural intricacies of expansive clay.

2.6. X-Ray Diffraction. XRD is a potent technique employed for the identification of distinct mineral components within materials. In the scope of XRD testing, particles finer than 75 μm were utilized. The XRD pattern was meticulously recorded via an X-ray diffractometer utilizing CuKα radiation ($\lambda = 1.5406$ Å), while scanning across a diffraction angle 2θ spanning from 10° to 80°, with increments of $2\theta = 0.02°$. This rigorous process culminated in the acquisition of diverse phases within each material, discerned through the careful analysis of peaks present within the XRD patterns, facilitated by the employment of the X-Pert High Score software tool.

2.7. Scanning Electron Microscope. The SEM stands as a formidable analytical tool, wielding the capacity to meticulously examine an array of materials at elevated magnifications, yielding high-resolution images that unveil intricate details. In the context of this study, SEM assumes the role of characterizing the microstructure and surface morphology of the natural soil specimen, as well as providing a qualitative insight into the evolving microstructural intricacies within the matrix of the stabilized soil specimens.

3. Results and Discussion

3.1. Effect of ESA on Swelling Behavior. Figure 7 presents a graphical representation of the influence of varying concentrations of ESA on the FSI of the expansive clay. Evidently, the incremental addition of ESA at rates of 2%, 4%, 6%, and 8% exerts a notable impact on the swelling tendencies of the natural soil. Specifically, the incorporation of ESA leads to a progressive reduction in the swelling propensity of the soil, culminating in FSI values of 60%, 45.45%, 40.91%, and 36.36%, respectively, from the initial value of 95%. This noteworthy trend underscores the compelling effectiveness of ESA in mitigating the swelling characteristics inherent to expansive clay. It becomes evident that the optimal concentration of 6% ESA engenders a marked improvement in the swelling potential of the soil sample, substantiating ESA's role in ameliorating the expansive tendencies of the clay.

3.2. Effect of ESA on Index Properties. Figure 8 portrays the plasticity and shrinkage characteristics exhibited by stabilized soil with ESA. Notably, the introduction of ESA induces discernible alterations in the soil's properties. This is notably evidenced by a reduction in the liquid limit, accompanied by

Table 3: Mix design considered for laboratory tests.

Sample	Natural soil (%)	ESA (%)	SP (%)
Soil	100	0	0
Expansive clay + ESA	98	2	0
	96	4	0
	94	6	0
	92	8	0
Expansive clay + ESA + SP	89	Optimum amount of ESA (6%) was used throughout this stage	5
	84		10
	79		15
	74		20

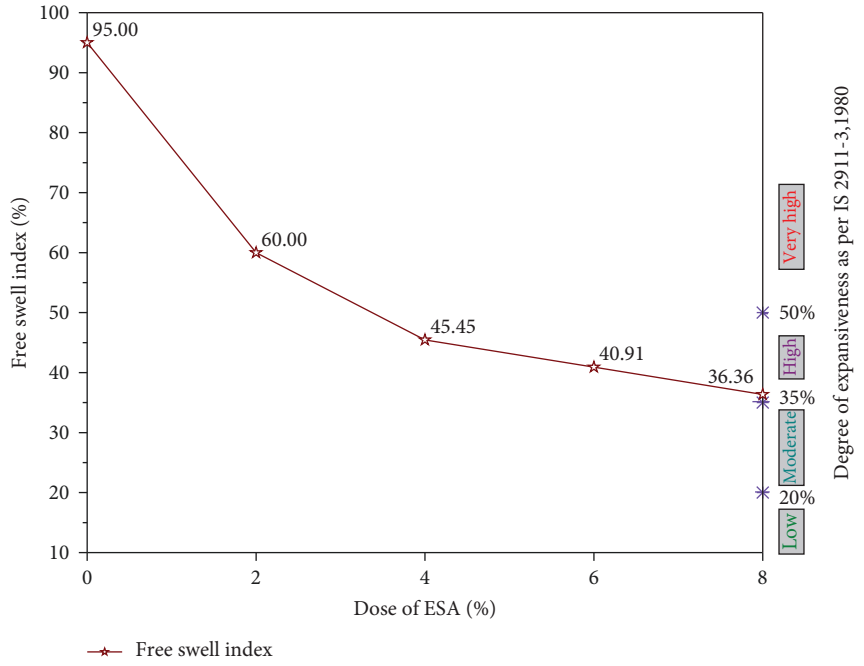

Figure 7: Influence of eggshell ash dose on FSI of soil.

an augmentation in the plastic limit, thereby leading to a commensurate decrease in the PI of the natural soil. The inclusion of 8% ESA, for instance, brings about a noteworthy decline in the soil's liquid limit, lowering it from 84.38% to 78.23%. Concurrently, the plastic limit undergoes an increment from 37.22% to 45.58% upon the inclusion of 8% ESA in the sample. The amalgamation of these effects manifests in the form of a diminished PI, dropping from an initial 47.16% to 32.65% at the 8% ESA concentration. This phenomenon is attributed to the interaction between the liberated Ca^{2+} ions from ESA and the adsorbed cations of the clay mineral. This interaction triggers a reduction in the diffused water layer surrounding clay particles. Consequently, the proximity between these particles increases, culminating in the aggregation or flocculation of clay particles. The cumulative impact translates into a perceptible reduction in the plasticity behavior of the expansive soil, aligning with observations from the previous research [18, 26–28]. The progressive decrease in the plasticity index, in tandem with rising ESA content, underscores ESA's propensity to promote clamping, flocculation, and coarsening of the soil particles.

3.3. Effect of ESA on Compaction Characteristics. Figure 9 presents the compaction curve detailing the behavior of the soil sample infused with ESA at various concentrations of 2%, 4%, 6%, and 8% by dry weight of soil. A discernible trend emerges, reflecting changes in the MDD and OMC of the treated sample. Remarkably, the incorporation of ESA triggers a reduction in the MDD of the treated sample, transitioning from an initial 1.32–1.27 g/cm^3 upon reaching the 8% ESA concentration. This drop can be attributed to the substitution of soil by ESA, which boasts a comparatively lower specific gravity when compared to the native soil. Conversely, the OMC of the treated sample displays a discernible increase, ascending from an initial value of 35.78%–38.32% with the inclusion of 8% ESA. This phenomenon stems from the heightened calcium content within the soil as a result of ESA introduction. Consequently, an augmented quantity of

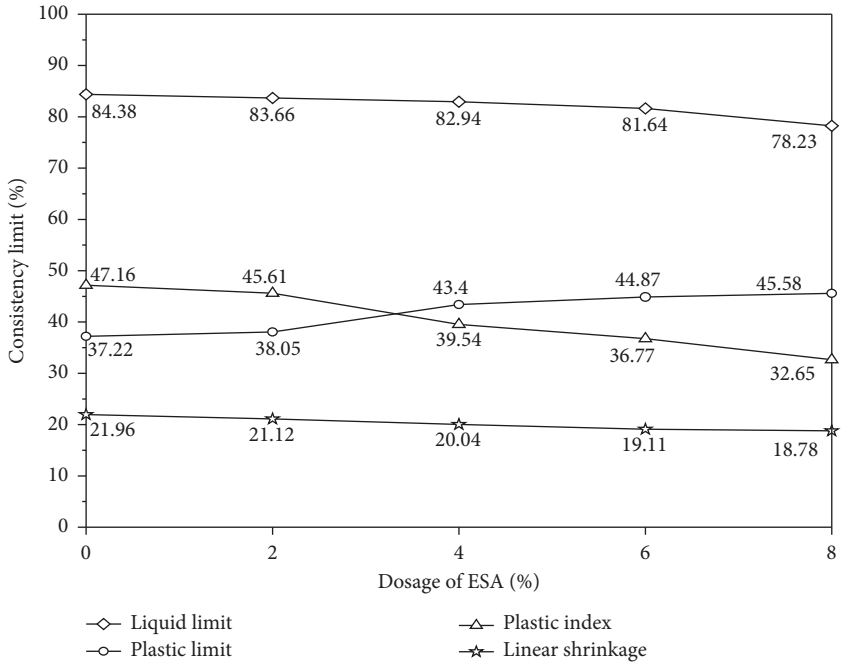

Figure 8: Variation of soil index values with ESA content.

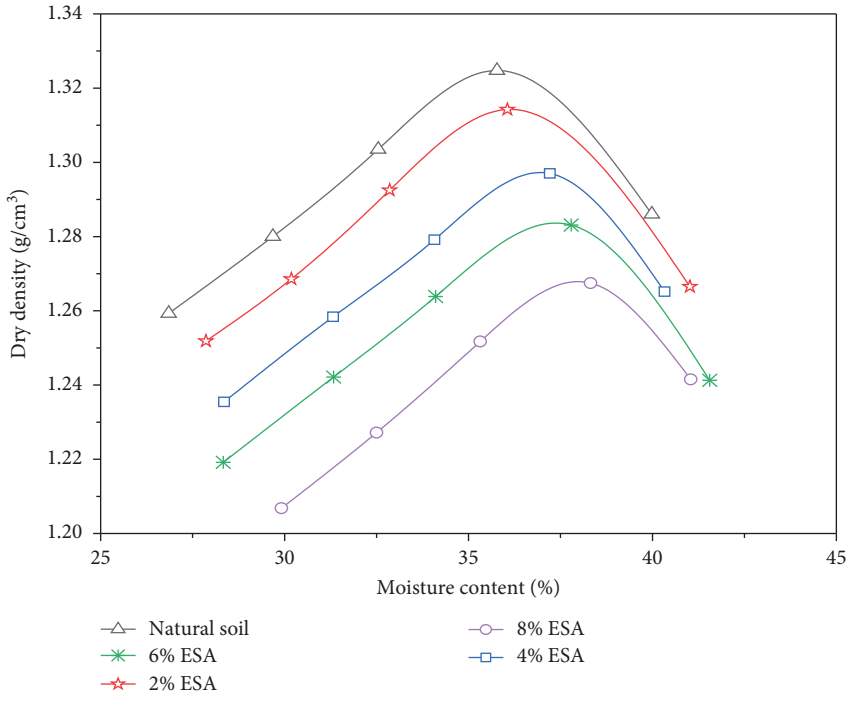

Figure 9: Compaction curve of soil mixed with eggshell ash.

water is necessitated to facilitate the hydration process and foster the formation of calcium silicate hydrate particles. Furthermore, the compaction curves denote an elevated water requirement for the initiation of chemical reactions among the fine particles, signifying the commencement of the stabilization process. This phenomenon is attributed to the significant CaO content present within the ESA, further emphasizing the role of high-calcium levels in influencing the compaction behavior and stabilization dynamics of the treated soil sample.

3.4. Effect of ESA on Compressive Strength. Figure 10 serves to depict the relationship between the UCS values and the varying concentrations of ESA when blended with expansive clay, observed under both uncured and cured conditions. A discernible trend is evident, showcasing how the UCS values

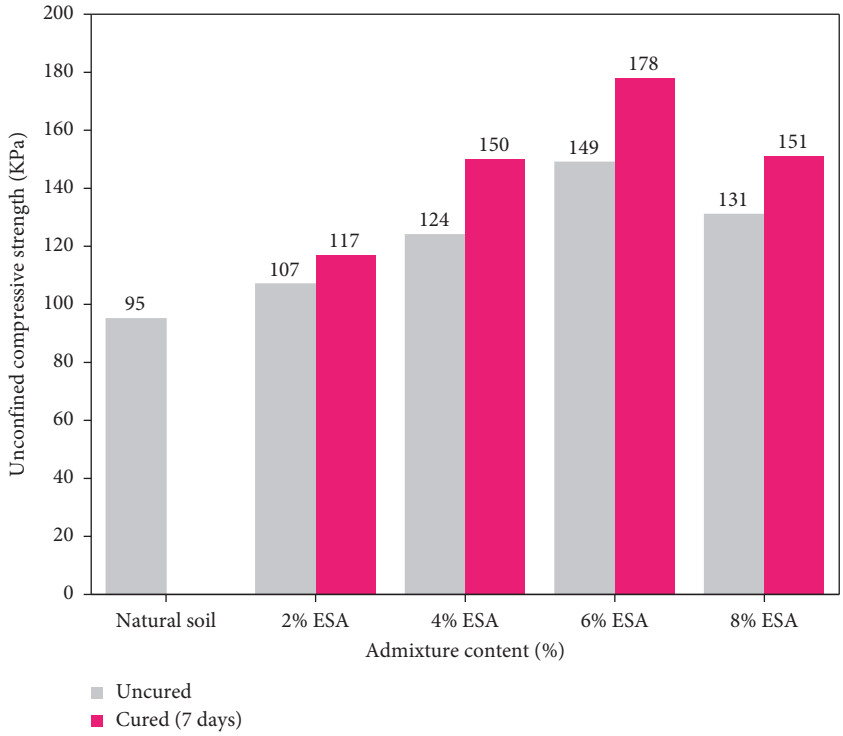

Figure 10: Influence of ESA on unconfined compressive strength.

evolve in response to the ESA content. Remarkably, the UCS experiences an incremental enhancement as the ESA concentration rises, culminating in a notable increase up to the 6% ESA content. However, at the 8% ESA concentration, the UCS value exhibits an anticipated decline. This observed decrease can be attributed to the emergence of a cohesionless soil structure, resulting from the interaction between the ESA minerals and the soil matrix. Furthermore, the impact of curing time on the UCS values is a noteworthy consideration, underlining the influential role of the additive's pozzolanic nature. This pozzolanic characteristic triggers significant changes in the compressive strength dynamics, as evident in Figure 10.

3.5. Combined Effect of SP and ESA. In the ensuing phase of this investigation, the focus shifted to examining the impact of SP on the behavior of expansive clay, with the concentration of ESA consistently maintained at 6%. Accordingly, the analyses were conducted by manipulating the concentration of SP while maintaining a constant 6% ESA content.

3.5.1. Effect of SP and ESA on Swelling Behavior. Figure 11 illustrates the relationship between the content of SP and the corresponding FSI percentage of the natural soil. The introduction of varying SP concentrations at 5%, 10%, 15%, and 20% to the initially treated soil yields a successive reduction in the FSI, yielding values of 33.33%, 31.15%, 28.57%, and 22.73%, respectively. Notably, the most compelling impact is observed at the 20% SP content, resulting in a noteworthy enhancement of soil performance. This conspicuous improvement is especially significant, as the addition of 20% SP to the initially treated soil sample effectively mitigates swelling tendencies, resulting in a classification within the low degree of expansion category. Evidently, the synergistic interaction between ESA and SP demonstrates an even more pronounced capacity for reducing the swelling characteristics inherent in expansive clay. These findings align harmoniously with analogous outcomes in previous studies, as demonstrated by the works of Jain et al. [29], Bapiraju and Prasad K [18], Blayi et al. [20], and Carlina et al. [28].

3.5.2. Effect of SP and ESA on Index Properties. Figure 12 exemplifies the discernible impact of SP on the index properties of expansive clay. Notably, the introduction of SP at varying concentrations (5%, 10%, 15%, and 20%) yields appreciable transformations in the liquid limit and plastic limit, causing a decline from 76.55% to 71.91% and 43.12% to 40.23%, respectively. Moreover, this additive-induced alteration echoes in the PI, effectively diminishing it from 33.43% to 31.68%. A similar trend is noted in the linear shrinkage property, wherein the natural clay initially mixed with 6% ESA exhibits a substantial reduction in linear shrinkage, plummeting from 17.81% to 12.62% upon incorporation of the same proportion of SP. This collective array of findings provides unequivocal affirmation that the introduction of SP serves as an effective modulator, adept at attenuating the index properties of expansive clay. This outcome is rooted in the distinctive nonplastic behavior exhibited by SP, underscoring its limited affinity for water absorption, an attribute that decisively contributes to the observed reductions in the index properties.

3.5.3. Effect of SP and ESA on Compaction Characteristics. Figure 13 shows the compaction curve of the soil sample mixed with 6% ESA and varied concentration of SP (i.e.,

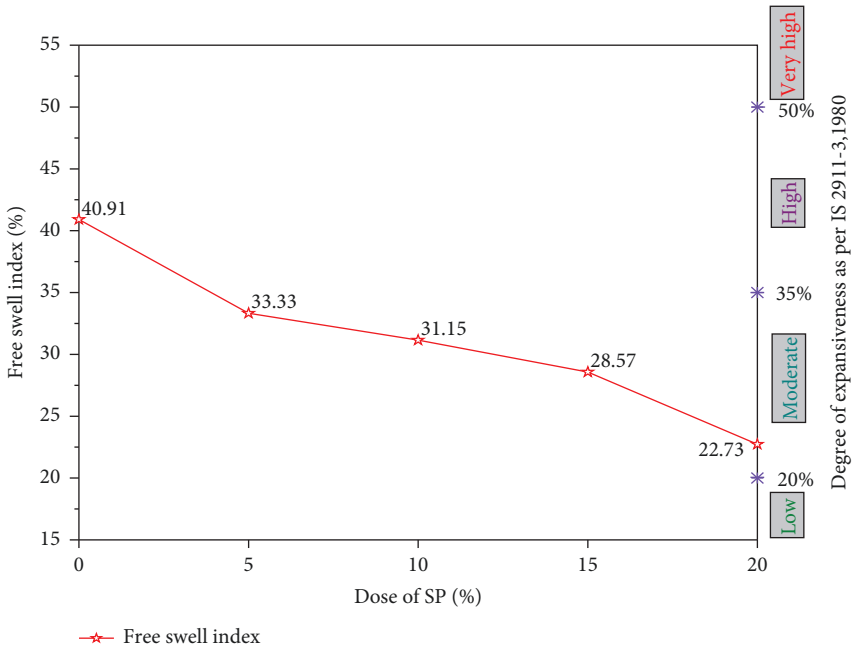

Figure 11: Variation of swelling index of soil with 6% ESA and variable SP content.

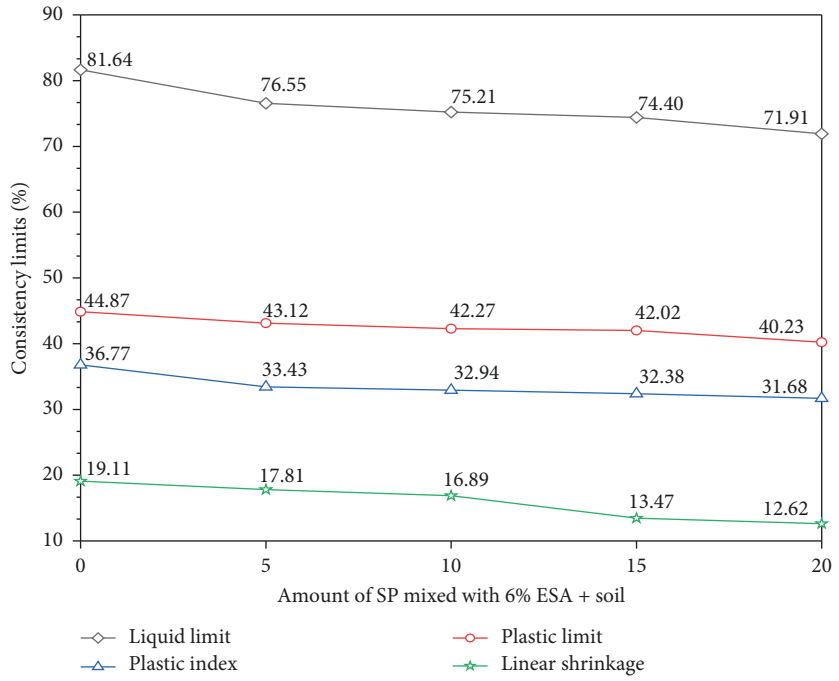

Figure 12: Effect of SP on index properties of expansive clay mixed with 6% ESA.

5%, 10%, 15%, and 20%) by dry weight of sample. It has been clearly seen that MDD of the treated sample increased from 1.30 to 1.38 g/cm^3 at 5% addition of SP content and further increased to 1.39 and 1.40 g/cm^3 for 10% and 15% of SP content, respectively. The reason for increment of maximum dry density of soil when increasing the content of SP was due to the replacement of clay with SP material, having higher specific gravity (i.e., $G_s = 2.78$). The OMC of the treated sample decreased from 37.79% to 36.09% when 5% SP is added to the soil. In addition, when 20% SP is applied, the OMC is reduced to 33.93%. This behavior is expected because the clay content of the natural soil has been replaced with SP which has less attraction to water molecules [18, 20]. Figure 13 provides a compelling illustration of the compaction curve, tracing the behavior of the soil sample infused with 6% ESA and varying concentrations of SP (5%, 10%, 15%, and 20%) measured by dry weight of the sample. The discernible trend unveils intriguing insights into the evolution

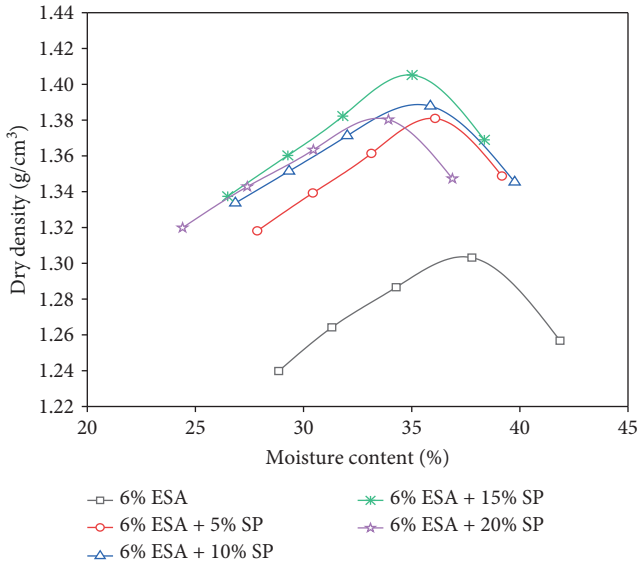

Figure 13: Compaction behavior of soil treated with stone powder.

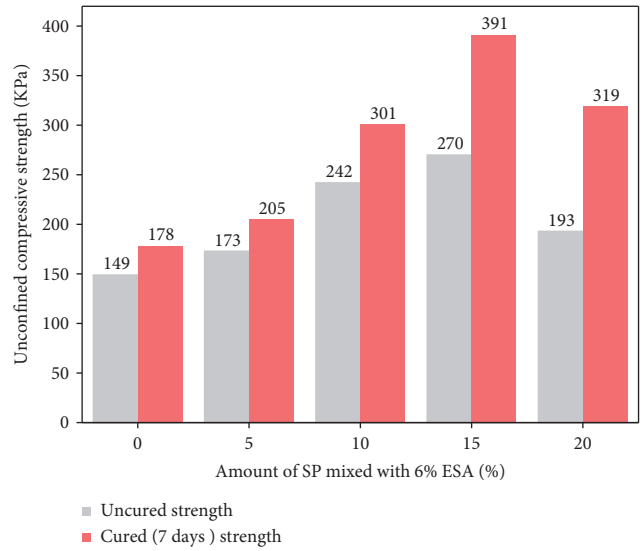

Figure 14: Effect of mixing variable SP on UCS of natural clay.

of the MDD and OMC of the treated sample. Clearly evident is the progressive augmentation of MDD in response to the introduction of SP content. For instance, at a mere 5% SP addition, the MDD escalates from 1.30 to 1.38 g/cm^3. This trend continues with a subsequent increase to 1.39 g/cm^3 for 10% SP content, and further to 1.40 g/cm^3 for 15% SP content. This observed rise in MDD can be attributed to the replacement of clay by the SP material, notable for its higher specific gravity $G_s = 2.78$. Conversely, the OMC of the treated sample undergoes a distinctive shift. Upon introducing 5% SP to the soil, the OMC contracts from 37.79% to 36.09%. Notably, the addition of 20% SP yields a notable reduction, driving the OMC down to 33.93%. This behavior is in line with expectations, as the substitution of clay content with SP, characterized by lower affinity for water molecules, underpins this observed decline. This phenomenon resonates with findings reported by Bapiraju and Prasad K [18] and Blayi et al. [20], further underlining the congruence between observed behaviors and prior research in this domain.

3.5.4. Effect of SP and ESA on Compressive Strength Behavior. Figure 14 presents the dynamic evolution of the uniaxial compressive strength in natural soil, intricately influenced by the varying concentration of SP under 6% ESA content, considered within both uncured and cured conditions. Notably, the UCS in natural soil, when imbued with 6% ESA, manifests as 149 kPa for uncured and 178 kPa for cured conditions. The UCS values exhibit a distinct trajectory, echoing the nuances of SP concentration. At 5% SP content, the UCS value escalates to 173 kPa, while a more substantial progression is observed at 10%, yielding 242 kPa. Similarly, concentrations of 15% and 20% register 270 and 193 kPa, respectively. The anticipated reduction in UCS at 20% SP can be attributed to the accompanying decline in soil cohesive property. A noteworthy revelation is the tangible enhancement in UCS witnessed under 7-day curing conditions, as depicted

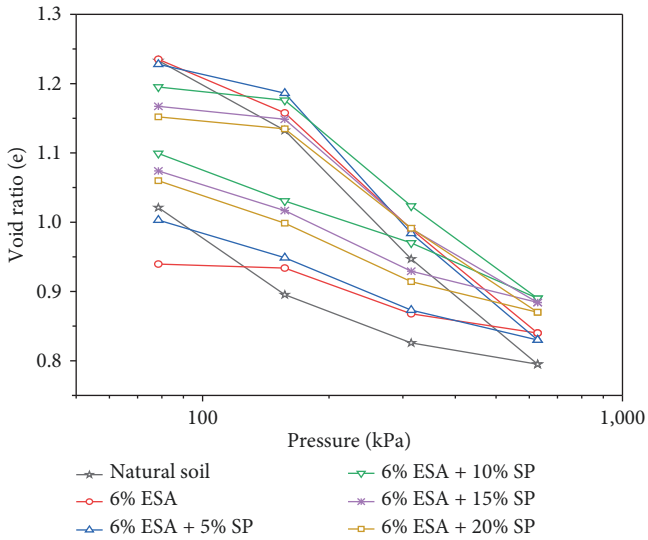

Figure 15: Variation of void ration vs. pressure.

in Figure 14. This augmentation in strength can be attributed to a convergence of mechanisms due to cation exchange, flocculation, and the pozzolanic reaction between the additives and clay minerals. This phenomenon harmonizes with observations from previous research, as detailed by Sivrikaya et al. [22] and Blayi et al. [20], which demonstrated the propensity of SP to diminish cohesive properties, thereby enriching the soil's overall strength profile.

3.6. Effect of ESA and SP on Compressibility Parameters. The impact of varying SP concentration on soil compressibility behavior has been meticulously investigated. Illustrations in Figure 15 are the curves mapping of initial void ratio against pressure on logarithmic scale across different SP concentrations. Notably, a discernible trend emerges, underscoring a consistent reduction in the initial void ratio as the concentration of additives increases (Table 4).

Table 4: Summary of consolidation result and compression parameters of specimens.

Cases	Pressure (kPa)	Sample type					
		S	E6-S	E6-C5-S	E6-C10-S	E6-C15-S	E6-C20-S
e (loading)	0	1.29	1.27	1.26	1.22	1.19	1.17
	78	1.23	1.24	1.23	1.20	1.17	1.15
	156	1.13	1.16	1.19	1.18	1.15	1.14
	312	0.95	0.99	0.98	1.02	0.99	0.99
	624	0.80	0.84	0.83	0.89	0.88	0.87
e (unloading)	78	1.02	0.94	1.00	1.10	1.07	1.06
	156	0.90	0.93	0.95	1.03	1.02	1.00
	312	0.83	0.87	0.87	0.97	0.93	0.91
	624	0.80	0.84	0.83	0.89	0.88	0.87
C_c		0.62	0.56	0.51	0.51	0.45	0.40
e_o		1.29	1.27	1.26	1.22	1.19	1.17
Average m_v (Mpa^{-1})		0.40	0.33	0.30	0.22	0.21	0.20

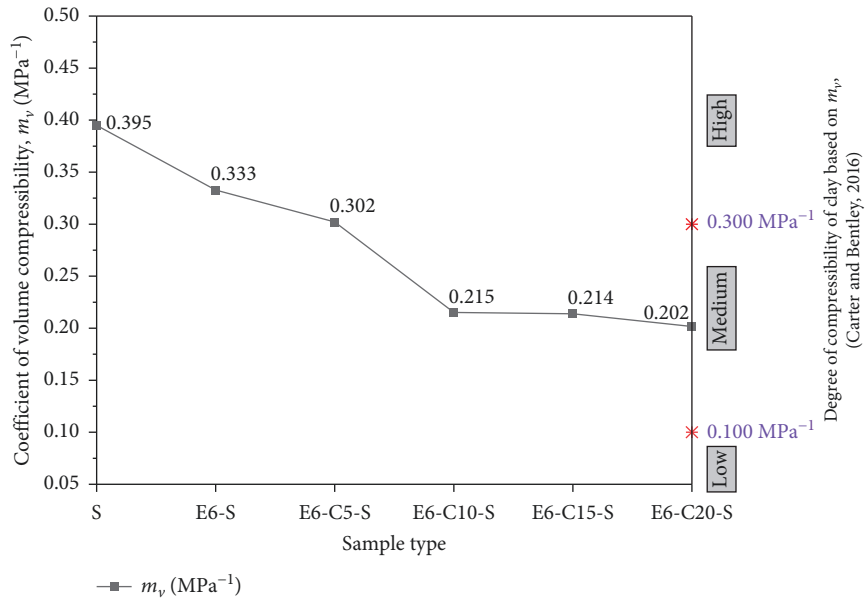

Figure 16: Coefficient of volume compressibility of soil variation with dose of additives.

The initial void ratio of the natural soil exhibited a notable decrease, diminishing from 1.29 to 1.17, as a result of a 6% ESA concentration combined with 20% SP content. This reduction in e_o finds its origin in the moisture content reduction attributed to the escalated percentage of SP. Furthermore, the compression index (C_c) of the soil manifests a tangible decline, receding from 0.62 to 0.40, mirroring the increasing SP concentration at a constant 6% ESA content. This diminution in the compressibility index is a direct consequence of the replacement of expansive clay with nonplastic material, characterized by either limited or absent swelling tendencies. As a consequence, the soil sample experiences a qualitative shift, marked by a decreased compressibility index, an outcome precipitated by the infusion of nonplastic components.

Furthermore, as depicted in Figure 16, the fluctuation in the coefficient of volume compressibility with in soil samples enriched with 6% ESA and varying SP concentrations is unveiled. The outcomes underscore a noteworthy trend, showcasing a compelling reduction in the coefficient of volume compressibility values. Specifically, the values dwindle from 0.40 to 0.20 MPa^{-1} equivalent to a remarkable 48.86% decrease when the SP concentration reaches 20% while ESA remains constant at 6%. This decline in the coefficient of volume compressibility owes its origin to the heightened concentration of additives (ESA and SP), engendering a discernible reduction in compressibility behavior. This observation parallels findings elucidated by Mohanty et al. [30], who similarly reported a diminishing coefficient of volume compressibility with an escalating percentage of fly ash up to 30%. The collective evidence substantiates the efficiency of the proposed additives in tempering the compressibility characteristics of the soil samples.

Table 5: Summary of coefficient of consolidation of samples with varying additives.

Pressure (kPa)	Coefficient of consolidation, (C_v) (m^2/year)					
	S	E6-S	E6-C5-S	E6-C10-S	E6-C15-S	E6-C20-S
78	2.00	2.02	2.07	2.13	2.17	2.27
156	1.70	1.74	1.80	1.84	1.93	1.96
312	0.97	1.02	1.05	1.11	1.18	1.21
624	0.41	0.42	0.43	0.48	0.48	0.50
Average C_v	1.27	1.30	1.34	1.39	1.44	1.49

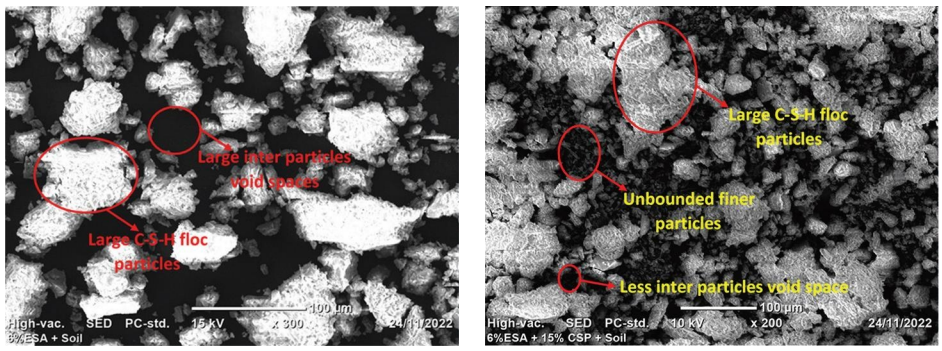

(a) (b)

Figure 17: SEM photograph (a) 6% ESA + soil and (b) 6% ESA + 15% SP + soil.

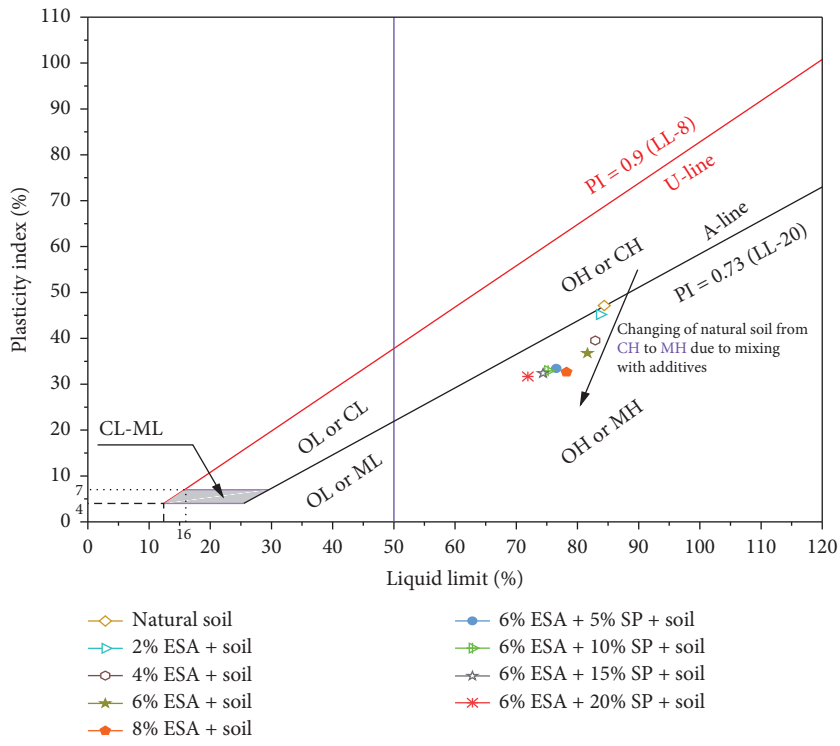

Figure 18: Plasticity chart showing effect of additives on soil group.

The coefficient of consolidation (C_v) exhibits a discernible pattern, lowering from 2.00 to 0.41 m^2/year, as the pressure escalates from 78 to 624 kPa (Table 5). This trend highlights the noteworthy relationship between the pressure increment and the elongation of the time span requisite for the soil to attain a 50% degree of consolidation, indicating an augmentation in the time frame as the effective stress intensifies. Furthermore, an intriguing observation emerges,

elucidating the average value of C_v, which undergoes a transition from 1.27 to 1.49 m^2/year. This shift occurs when the natural soil is blended with 20% CSP and 6% ESA. The underlying rationale for this shift lies in the heightened content of additives within the blended soil samples, ultimately leading to a reduction in the plasticity characteristics of these composite samples. This finding aligns seamlessly with analogous outcomes from a prior study, as documented by Mohanty et al. [30], further reaffirming the consistency and validity of the observed trends.

Figure 17 presents the SEM image results, offering a visual glimpse into the microstructural shifts introduced by the addition of (a) 6% ESA alone, and (b) the combined infusion of 6% ESA and 15% SP within the expansive clay matrix. Upon closer examination, a discernible divergence from the natural expansive clay composition becomes evident, characterized by the presence of coarser particles. Notably, the formation of these coarser grains finds its underpinning in the particle floc formation mechanism, a product of the pozzolanic reaction spurred by the interaction between cations derived from ESA and the soil matrix. Delving into the second image (b), a striking interplay between coarser and finer particles unfolds within the soil sample infused with 6% ESA and 15% SP. Once again, coarser particles emerge as a result of the aforementioned particle floc formation process, akin to the first case. In tandem, the presence of finer particles is observed, presumably arising from the introduction of additional SP particles. This dual presence of coarser and finer particles in the microstructure of the soil sample accentuates the intricate interplay between the additives and the expansive clay, further corroborating the transformative impact of these additives on the microstructural composition (Figure 18).

4. Conclusions

The investigation into the influence of ESA and SP on the geotechnical and microstructural behavior of expansive clay has yielded valuable insights. The experimental approach encompassed an initial blending of the natural soil with varying ESA concentrations (2%, 4%, 6%, and 8%), followed by the addition of SP at concentrations of 5%, 10%, 15%, and 20%, thereby examining the combined impact of these additives on the expansive clay. Drawing upon the outcomes of laboratory analyses, the following conclusions have been established:

(1) The incorporation of 8% ESA by dry weight engenders a discernible reduction in the FSI, PI, and linear shrinkage. These findings underscore the efficacy of ESA in mitigating expansive and shrinkage tendencies within the expansive clay.

(2) At a concentration of 6% ESA, a notable enhancement in the UCS is witnessed; escalating from 95 to 149 and 178 kPa for uncured and 7 days cured conditions, respectively.

(3) Subsequent addition of SP to the initially treated soil (soil + 6% ESA + SP) elicits improvements in index properties and a reduction in swelling behavior.

(4) The introduction of 6% ESA and 20% SP to the natural expansive clay augments the maximum dry density of the sample from 1.30 to 1.38 g/cm^3, while simultaneously reducing the optimum moisture content from 37.79% to 33.93%.

(5) The optimal mix, as determined by this experimental study, converges at a composition of 6% ESA and 15% SP. Notably, this blend propels the compressive strength of the soil sample to increase from 149 to 270 kPa for uncured conditions, and from 178 to 391 kPa for 7 days cured conditions, unveiling the affirmative impact of curing on material strength.

(6) Ultimately, the amalgamation of 6% ESA and 15% SP with the natural soil emerges as the optimal composition, delivering a dual enhancement in both microstructural attributes and mechanical properties, effectively fortifying the inherent characteristics of the natural soil.

Abbreviations

AASHTO: American Association of State, Highway and Transport Official
ASTM: American Society for Testing Material
BS: British standard
C-S-H: Calcium silicate hydrate compound
C_V: Coefficient of consolidation
m_v: Coefficient of volume compressibility
C_c: Compressibility index
ESA: Eggshell ash
FSI: Free swell index
FSR: Free swell ratio
JCPDS: Joint committee on powder diffraction standards
LL: Liquid limit
LOI: Loss of ignition
MDD: Maximum dry density
OMC: Optimum moisture content
PI: Plastic index
PL: Plastic limit
SEM: Scanning electron microscope
SP: Stone powder
UCS: Unconfined compressive strength
USCS: Unified soil classification system
XRD: X-ray diffraction.

Data Availability

The data sets used and/or analyzed during the current study are available from the corresponding author upon reasonable request.

Additional Points

Limitations and Future Works. In this study, the calcination temperature of eggshell was deliberately confined to 650 ± 25°C. However, it is recommended that future investigations explore a wider range of incineration temperatures to

ascertain their impact on eggshell properties. Furthermore, the scope of this study predominantly focused on the individual mineralogical characterization of the soil and the two additives. However, it is worth noting that future research endeavors could encompass the comprehensive characterization of the combined soil-additive matrix. The evaluation of compressive strength in this research was constrained to a 7-day curing period. To enhance the understanding of the temporal evolution of strength properties facilitated by ESA and SP admixtures, it is suggested that extended investigations be conducted to assess the influence of varying curing durations.

Conflicts of Interest

This study involves no conflicts of interest between authors.

Acknowledgments

This study did not receive any funds but is a part of the employer at Adama Science and Technology University. The authors would like to express their gratitude to the Adama Science and Technology University, Civil Engineering Department for giving access to laboratory facilities to execute this research.

References

[1] S. Vorwerk, D. Cameron, and G. Keppel, "Clay soils in suburban environments: movement and stabilization through vegetation," in *Ground Improvement Case Histories Chemical, Electrokinetic, Thermal and Bioengineering*, B. Indraratna, J. Chu, and C. Rujikiatkamjorn, Eds., pp. 655–682, Elsevier, 2015.

[2] M. K. Atahu, F. Saathoff, and A. Gebissa, "Strength and compressibility behaviors of expansive soil treated with coffee husk ash," *Journal of Rock Mechanics and Geotechnical Engineering*, vol. 11, no. 2, pp. 337–348, 2019.

[3] P. S. Reddy, B. Mohanty, and B. H. Rao, "Influence of clay content and montmorillonite content on swelling behavior of expansive soils," *International Journal of Geosynthetics and Ground Engineering*, vol. 6, Article ID 1, 2020.

[4] J. D. Nelson and D. J. Miller, *Expansive Soils: Problem and Practice in Foundation and Pavement Engineering*, Wiley, New York, 1992.

[5] H. Canakci, A. Aziz, and F. Celik, "Soil stabilization of clay with lignin, rice husk powder and ash," *Geomechanics and Engineering*, vol. 8, no. 1, pp. 67–79, 2015.

[6] U. Zada, A. Jamal, M. Iqbal et al., "Recent advances in expansive soil stabilization using admixtures: current challenges and opportunities," *Case Studies in Construction Materials*, vol. 18, Article ID e01985, 2023.

[7] F. A. Yitagesu, F. van der Meer, H. van der Werff, and W. Zigterman, "Quantifying engineering parameters of expansive soils from their reflectance spectra," *Engineering Geology*, vol. 105, no. 3-4, pp. 151–160, 2009.

[8] S. Y. Aga, "Physical stabilization of expansive subgrade soil using locally produced geogrid material," *SN Applied Sciences*, vol. 3, no. 5, Article ID 568, 2021.

[9] A. Tamrat, "*Study on index properties and swelling pressure of expansive soils found in Dukem*," *Geotechnical Engineering in Department of Civil Engineering*, MSc. Thesis, Addis Ababa Institute of Technology (AAiT), 2013.

[10] F. H. Chen, *Foundations on Expansive Soils*, Elsevier Science, New York, 1988.

[11] R. S. Rollings, J. P. Burkes, and M. P. Rollings, "Sulfate attack on cement stabilized sand," *Journal of Geotechnical and Geoenvironmental Engineering*, vol. 125, no. 5, pp. 364–372, 1999.

[12] Q. Chen and B. Indraratna, "Shear behavior of sandy silt treated with lignosulfonate," *Canadian Geotechnical Journal*, vol. 52, no. 8, pp. 1180–1185, 2015.

[13] L. C. Dang and H. Khabbaz, "Shear strength behavior of bagasse reinforced expansive soil," in *International Conference on Geotechnical and Earthquake Engineering*, pp. 393–402, IACGE, Chongqing, China, 2018.

[14] S. Y. Amakye and S. J. Abbey, "Understanding the performance of expansive subgrade materials treated with non-traditional stabilizers: a review," *Cleaner Engineering and Technology*, vol. 4, Article ID 100159, 2021.

[15] D. Neguse, E. Assefa, and S. M. Assefa, "Study on the performance of expansive subgrade soil stabilized with enset ash," *Advances in Civil Engineering*, vol. 2023, Article ID 7851261, 12 pages, 2023.

[16] M. N. J. Alzaidy, "Experimental study for stabilizing clayey soil with eggshell powder and plastic wastes," *IOP Conference Series: Materials Science and Engineering*, vol. 518, no. 2, Article ID 022008, 2019.

[17] N. S. Surjandari, N. Djarwanti, and N. U. Ukoi, "Enhancing the engineering properties of expansive soil using bagasse ash," *Journal of Physics: Conference Series*, vol. 909, no. 1, Article ID 012068, 2017.

[18] P. Bapiraju and N. Prasad K, "An experimental investigation on expansive soil in conjunction with eggshell powder and rock dust," *International Journal of Advanced Research in Engineering and Technology*, vol. 10, no. 5, pp. 9–21, 2019.

[19] F. M. Tchuente, H. K. Tchakouté, C. Banenzoué et al., "Microstructural and mechanical properties of (Ca, Na)-poly (sialate-siloxo) from metakaolin as alumino-silicate and calcium silicate from precipitated silica and calcined chicken eggshell," *Construction and Building Materials*, vol. 201, pp. 662–675, 2019.

[20] R. A. Blayi, A. F. H. Sherwani, F. H. R. Mahmod, and H. H. Ibrahim, "Influence of rock powder on the geotechnical behaviour of expansive soil," *International Journal of Geosynthetics and Ground Engineering*, vol. 7, no. 1, Article ID 14, 2021.

[21] R. B. Saldanha, C. G. Da Rocha, A. Lotero, and N. C. Consoli, "Technical and environmental performance of eggshell lime for soil stabilization," *Construction and Building Materials*, vol. 298, Article ID 123648, 2021.

[22] O. Sivrikaya, F. Uysal, A. Yorulmaz, and K. Aydin, "The efficiency of waste marble powder in the stabilization of fine-grained soils in terms of volume changes," *Arabian Journal for Science and Engineering*, vol. 45, pp. 8561–8576, 2020.

[23] A. Behnood, "Soil and clay stabilization with calcium—and non-calcium-based additives: a state-of-the-art review of challenges, approaches and techniques," *Transportation Geotechnics*, vol. 17, pp. 14–32, 2018.

[24] P. Solanki and M. Zaman, "Microstructural and mineralogical characterization of clay stabilized using calcium-based stabilizers," in *Scanning Electron Microscopy*, V. Kazmiruk, Ed., IntechOpen, Rijeka, Article ID 31, 2012.

[25] AASHTO M 145, "Classification of soil and soil-aggregate mixtures for highway construction purposes," 91, 2008.

[26] J. James and P. K. Pandian, "Bagasse ash as an auxiliary additive to lime stabilization of an expansive soil: strength and microstructural investigation," *Advances in Civil Engineering*, vol. 2018, Article ID 9658639, 16 pages, 2018.

[27] W. Diana, A. Widianti, and E. Hartono, "The strength behavior of eggshell powder substitution on soil–lime stabilization," *IOP Conference Series: Materials Science and Engineering*, vol. 1144, no. 1, Article ID 012089, 2021.

[28] M. Carlina, Y. Apriyanti, and F. Fahriani, "The effect of addition of bagasse ash and eggshell powder on CBR value of clay soil," *IOP Conference Series: Earth and Environmental Science*, vol. 926, Article ID 012102, 2021.

[29] A. K. Jain, A. K. Jha, and Shivanshi, "Geotechnical behavior and micro-analyses of expansive soil amended with marble dust," *Soils and Foundations*, vol. 60, no. 4, pp. 737–751, 2020.

[30] S. K. Mohanty, P. K. Pradhan, and C. R. Mohanty, "Consolidation and drainage characteristics of expansive soil stabilized with fly ash and dolochar," *Geotechnical and Geological Engineering*, vol. 34, no. 5, pp. 1435–1451, 2016.